euspen's 26th International Conference & Exhibition, Krakow, PL, June 2026
www.euspen.eu

Thermal behavior analysis of a novel measurement system for precise displacement sensors calibration

Luka Čas, Bojan Ačko and Rok Klobučar

University of Maribor, Faculty of Mechanical Engineering, Laboratory for Production Measurement

luka.cas@um.si

Abstract

High-precision displacement sensors, typically inductive, capacitive or incremental, are widely used in dimensional metrology due to their sub-micrometer accuracy. Their increasing use in industrial and laboratory applications has created a clear need for traceable calibration methods. As the national holder of the length standard in Slovenia, the Laboratory for Production Measurement (MIRS/UM-FS/LTM) is responsible for ensuring traceability of length measurements in this field. To meet this need, we have initiated the development of a custom measurement system for calibration of precise displacement sensors up to 150 mm. As part of this development, we investigated the influence of thermal effects on structural deformations and their impact on calibration uncertainty especially, their contribution to geometric errors. Although environmental conditions in precise length measurement are typically controlled using climate chambers, even minor air temperature variations can cause micrometer-level deformations in calibration setups. Due to the lack of direct measurement methods to determine thermal deformations, this study focuses on evaluating their impact using finite element simulations. A CAD model of the mechanical structure was developed and analysed in ANSYS. The structure was exposed to thermal boundary conditions derived from real temperature measurements performed on the actual measurement system setup placed inside a controlled climate chamber. The TEMP 14 sensor system was used to acquire temperature data, using two air sensors and eight material sensors distributed on the structure. Measured air temperature fluctuations were approximated by mathematical functions using the least squares method, which served as boundary inputs in the simulations. Both static and transient thermal simulations were conducted, followed by structural analyses to determine resulting displacements. Results show that thermal stabilization of the structure in simulation occurred after approximately 4 hours, closely matching experimental measurements. The maximum thermal deformation occurred at the tip of the sensor mount and slightly exceeded 17 µm. The resulting displacement field was used to evaluate the change in the sensor's geometric alignment. Although the sensor was assumed to be perfectly aligned initially, thermal expansion introduced a cosine error on the order of $\mathrm{e}_{\cos\mathrm{T}} = 2.5 \cdot 10^{-10} \cdot L$ and caused a maximum axis displacement of approximately 10 µm. These findings form an important part of the ongoing development of a precision calibration system for displacement sensors.

Thermal deformation, Finite element analysis, Calibration, Precise displacement sensors, Length measurement

1. Introduction

High-precision displacement sensors, also known as transducers, are widely used in dimensional metrology due to their ability to measure very small displacements with sub-micrometer accuracy [1]. These sensors, typically contact-type, are commonly employed in advanced manufacturing, precise positioning, laboratory measurements and calibration systems (e.g. gauge block comparators) [2-4].

In recent years, the Slovenian National Laboratory for Length has observed an increasing demand for calibrations of high-precision displacement sensors. To meet this demand and fulfill our responsibility for traceable length measurements in the country, we started developing a novel measurement system for calibrating these sensors.

While the calibration of displacement sensors is relatively straightforward, the main challenge lies in achieving sufficiently low measurement uncertainty. This requires a clear identification and quantification of all error sources that may influence the measurement result, including thermally induced structural deformations.

Temperature variations can have a significant effect on length measurements, as even small changes can induce micrometer-level deformations in the measurement setup. To reduce these effects, most laboratories rely on climate-controlled environments [5, 6] and temperature monitoring using sensors, combined with compensation techniques to correct for thermal expansion. Because such temperature controlled chambers with very high stability can be very expensive, metrology laboratories have increasingly explored alternative approaches for compensating temperature induced measurement errors.

With recent advances in simulation software, finite element analysis (FEA) is increasingly used to predict structural responses to applied loads, particularly in mechanical engineering. Most studies, where FEA were used to assess thermal errors in production engineering have been performed on CNC machines tools [7, 8] and hydraulic presses [9].

Despite its growing adoption, applications in high-precision dimensional metrology remain relatively rare. However, studies that have applied FEA in this field [10, 11] demonstrate its potential to accurately predict thermally and mechanically induced deformations, supporting its use in evaluating calibration uncertainties.

In this study, we investigated how our new system, constructed from commercially available components, behaves under controlled temperature conditions in our climatic chamber. We studied the influence of temperature on structural expansions and the resulting geometric errors of the calibrated sensor. Due to the lack of direct measurement methods to determine these thermal deformations, we focused on evaluating their impact using finite element simulations.

2. Methods

The following methods detail the measurement setup, temperature monitoring and FEA used to assess thermal and structural effects.

2.1. Measurement system setup

The measurement system developed for calibrating high-precision displacement sensors consists of commercially available components assembled into a modular mechanical structure. At its core, the system consists of a displacement-generating mechanism and a modular set of elements forming the platform on which the sensor under calibration is mounted

The entire system is placed within a controlled laboratory chamber, providing active temperature regulation with ±0.1 °C stability and continuous humidity monitoring. Once fully developed, all calibrations will be conducted within this chamber to maintain consistent environmental conditions.

For the analysis, we focused exclusively on the portion of the structure that forms the mount for the sensor under calibration. The displacement-generating mechanism was not included in the simulations, as our primary interest lies in evaluating how thermal effects influence the geometric errors of the sensor itself.

To support the thermal analysis a CAD model of the measurement system was created in SolidWorks. Figure 1 shows the full prototype, with the outlined portion indicating the part of the system included in the analysis.

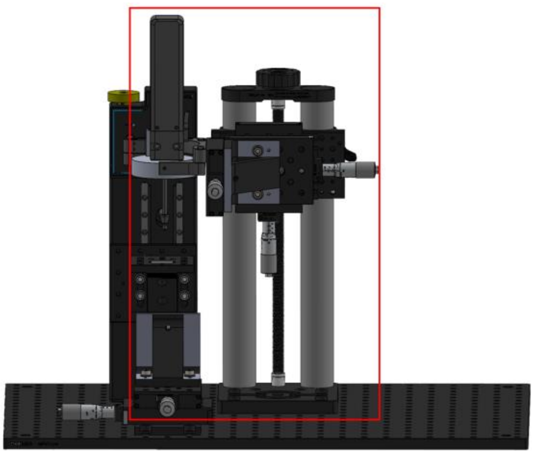

Figure 1. CAD model of the measurement system, showing the section included in simulations

The initial model, composed of six main components, was simplified to optimize meshing and solver efficiency while preserving the key stiffness, mass distribution, and thermal load paths. Components were positioned in their extreme operational configurations to define boundary conditions and ensure relevance for evaluating thermal effects on the sensor. The sensor itself was modelled at its maximum calibration length of 150 mm to capture the worst-case thermal deformation scenario.

2.2. Temperature Monitoring of the Measurement System

To determine the environmental conditions within the chamber, both air and material temperatures of the measurement system were continuously monitored using the TEMP 14 sensor system (JENAer Meßtechnik), which offers high precision with expanded calibration uncertainties of 15 mK for material sensors and 50 mK for air probes. The calibration of the system is traceable to the national temperature standard in Slovenia.

Eight material sensors were distributed across the structure, while two air sensors were placed at opposite ends of the base plate, separated by 0.6 m, to capture the overall temperature field, as shown in Figure 2. These measurements were used to define the boundary conditions for subsequent finite element simulations.

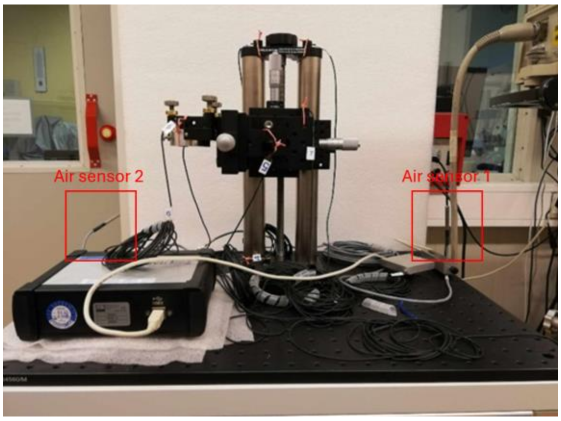

Figure 2. Placement of air and material sensors on the measurement system and monitoring under real chamber conditions.

Measurements began immediately after placing the system in the climatic chamber and continued for almost an entire day.

2.3. Temperature Approximation

To define the boundary conditions for the thermal analysis, the measured air temperature fluctuations in the chamber were approximated using a mathematical model. The measurements at the two air sensor positions along the base plate (T_1 at x = 0 m and T_2 at x = 0.6 m) were fitted to sinusoidal functions using the least squares method. For simplicity, the fluctuations were assumed to be in phase and to share the same frequency.

The general form of the fitted function was:

$$T(t) = A \cdot \sin(\omega t + \Phi) + T_0 \tag{1}$$

where:

- A – amplitude of the sinusoidal variation,
- ω – frequency of the sinusoidal variation,
- ϕ – phase shift of the sinusoidal variation,
- T_0 – mean temperature.

The fitted functions for the two measurement locations were:

$$T_1(t) = 0{,}03673 \cdot \sin(-0{,}005383 \cdot t + 1{,}865) + 19{,}593 \tag{2}$$

$$T_2(t) = 0{,}02935 \cdot \sin(-0{,}005008 \cdot t + 1{,}869) + 19{,}729 \tag{3}$$

Because both measured signals varied in phase and exhibited nearly identical frequency, the expressions were simplified by assuming a common frequency:

$$T_1(t) = 0{,}03673 \cdot \sin(-0{,}005 \cdot t) + 19{,}593 \tag{4}$$

$$T_2(t) = 0{,}02935 \cdot \sin(-0{,}005 \cdot t) + 19{,}729 \tag{5}$$

For the thermal analysis, the air temperature distribution along the length of the system was assumed to vary only in the x-direction, consistent with the sensor placement, while remaining constant in the y-direction due to the limited number of air sensors.

The temperature at any position x along the base plate was obtained by linear interpolation between $T_1(t)$ and $T_2(t)$:

$$T(x,t) = T_1 + (T_2 - T_1) \cdot (\frac{x-x_1}{x_2-x_1}) \tag{6}$$

Substituting the simplified expressions yields the final spatial- and time-dependent boundary condition:

$$T(x,t) = 19.593 + 0.03673 \cdot \sin(-0.005 \cdot t) + 0.2275 \cdot x - 0.01231 \cdot x \cdot \sin(-0.005 \cdot t) \tag{7}$$

The resulting spatial and time dependent function was then used as the boundary condition for the subsequent thermal deformation analysis of the sensor, capturing the measured environmental fluctuations in the chamber.

2.4. Simulation setup: materials and meshing

The finite element simulations were carried out in ANSYS using the simplified CAD model described earlier. The structure consists of four materials, with aluminium 6061-T6 as the primary one. Additional components are made from aluminium 7075-T6, AISI 1026 DOM steel and ferritic stainless steel. The model was discretized using ANSYS automatic mesh settings. A medium density mesh was selected after preliminary convergence checks, resulting in approximately 1.5 million nodes.

2.5. Thermal and Structural Analysis

A steady-state thermal analysis was first performed to determine the temperature field within the structure. The analysis assumes time-independent conditions, i.e., the system is in thermal equilibrium. The ambient temperature distribution was defined using a linear approximation obtained from the average readings of two air probes:

$$T(x) = 19.59 + 0.233\,x \tag{8}$$

Convective boundary conditions were applied to all exposed surfaces, while the bottom surface of the base plate was constrained to the measured granite temperature. The initial temperature of the model was set to 20 °C.

Based on the resulting temperature field, a static structural analysis was carried out to evaluate the thermally induced deformations. The temperature distribution from the thermal analysis was imported into the structural model. Gravity was applied as an additional load, and the base plate was fixed at its interface with the granite support.

A time-dependent thermal analysis was performed to evaluate the transient temperature evolution of the structure. The initial temperature of the entire model was set to 24 °C, representing the room temperature prior to cooling. Boundary conditions included the granite base temperature and convection applied to all exposed surfaces. In contrast to the steady-state analysis, the convection boundary was defined using the full temperature function from equation (7), which depends on both position and time. The duration of the simulation was set to 6 hours. This value was chosen based on experimental observations indicating that the system reaches thermal equilibrium after approximately 6 hours inside the climatic chamber, while still keeping the computational effort reasonable.

3. Results

This section presents thermal and structural analysis results, including their impact on sensor alignment, cosine, and Abbe errors.

3.1. Experimental results

The thermal behaviour of the system was evaluated through continuous temperature monitoring inside the climatic chamber. Measurements started immediately after the system was placed in the chamber and were recorded for nearly 24 hours. The structure reached thermal stabilization after approximately 6 hours, with the material sensors recording an average temperature of 19.9 °C and a maximum difference of 0.05 °C. Air temperature measurements showed periodic fluctuations at both ends of the base plate, which varied in phase, with maximum differences of 0.15 °C and 0.12 °C, respectively. The complete time evolution of both material and air temperatures is shown in Figure 3, illustrating the stabilization period and the characteristic behaviour of the air temperature fluctuations.

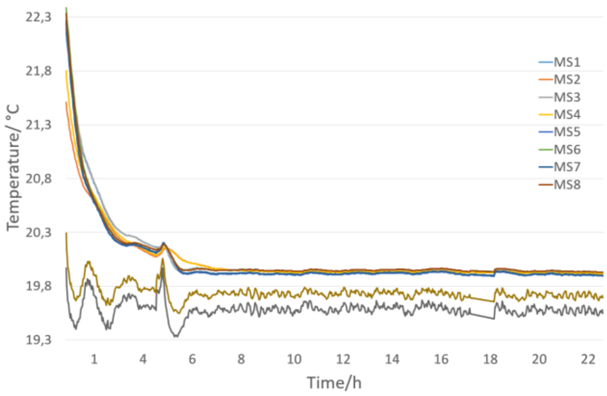

Figure 3. Temperature measurements of air and material sensors over time

3.2. Thermal and Structural Analysis Results

The steady-state thermal simulation provided the equilibrium temperature distribution along the structure. The maximum temperature (19.91 °C) occurred at the base plate in contact with the granite support, while temperatures decreased along the length, reaching a minimum of 19.65 °C at the top. Based on the resulting temperature field, static structural analysis showed maximum displacements of 17 µm at the sensor tip and rotational handle.

Time-dependent thermal simulations captured the evolution of the structure's temperature over 6 hours. The maximum temperature decreased from 24 °C and stabilized after approximately 4 hours, oscillating between 19.64 °C and 19.66 °C, while the minimum temperature remained near 19.91 °C. A summary of the simulation results, together with measured data from the real system, is presented in Table 1.

Table 1 Summary of ANSYS simulation results and measured data

Analysis Type	**ANSYS min**	**ANSYS max**	**Measured on real system**
Steady-state thermal	19.65 °C	19.91 °C	/
Steady-state structural	/	17.3 µm	/
Transient-thermal	19.64 °C	19.66 °C	/
Temp. stabilization	4 h		6 h

3.3. Geometric Errors Analysis

The resulting displacement field was used to evaluate the change in the sensor's geometric alignment. To evaluate the influence of structural deformations on the cosine error of the sensor stylus caused by temperature fluctuations, the ANSYS tip displacement data were post-processed in MATLAB. Two points at the ends of the 150 mm tip were tracked, and their displacements along the x and y axes were used to compute the resulting angular deviations from the initial alignment. The sensor was assumed to be initially perfectly aligned, with the cosine error set to zero.

The analysis, shown in Figure 4, indicates that the maximum angular deviations correspond to a cosine error of the sensor tip:

- x axis: $e_{\cos\mathrm{Tx}} = 2 \cdot 10^{-10} \cdot L$
- y axis: $e_{\cos\mathrm{Ty}} = 4 \cdot 10^{-11} \cdot L$

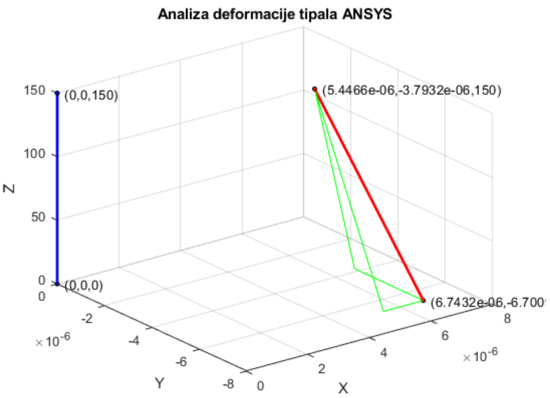

Figure 4. MATLAB analysis of sensor stylus angular deviations

The resulting combined cosine error along both axes (x and y) is approximately $e_{\cos\mathrm{T}} = 2.5 \cdot 10^{-10} \cdot L$. For comparison, the current laboratory capability allows aligning a 10 mm sensor stylus within an interval of approximately 3 µm, corresponding to a cosine error of $e_{\cos\mathrm{T}} = 10^{-7} \cdot L$.

To determine the Abbe error, between the sensor axis and the measurement axis of the reference laser beam positioned on the opposite side of the sensor, we performed an experiment measuring of pitch and yaw of the vertical stage. The largest measured angle was 8 µm/m, which corresponds to an Abbe error of 4 nm at the 0.5 mm offset of the axes. Thermal analysis indicated a maximum axis displacement of approximately 10 µm, which is negligible relative to the achievable 0.5 mm alignment.

Overall, the analysis demonstrates that temperature-induced deformations have a negligible impact on the sensor's geometric errors, including both cosine and Abbe errors.

4. Conclusion

A detailed investigation of the thermal and structural behaviour of the newly developed displacement sensor calibration system was performed using experimental measurements and finite element simulations. The results indicate that, under the tested temperature conditions, thermally induced deformations of the system have a negligible effect on the geometric accuracy of the sensor. Both the cosine and Abbe errors remain well below the laboratory's alignment capability. The analysis also confirms that the commercially available components and the overall modular assembly provide a mechanically and thermally stable structure. These findings support the use of the system for reliable and traceable sensor calibrations, without significant influence from temperature variations.

The ongoing work focuses on finalizing the automated calibration procedure, including the development and validation of calibration algorithms. Through further system optimization, additional reductions in measurement uncertainty are expected. The ultimate goal is to achieve an expanded uncertainty of 100 nm (*k* =2) over a 150 mm range, providing a fully automated, high-precision calibration capability for displacement sensors, thereby ensuring traceability for Slovenian accredited metrology laboratories and supporting the national industry.

5. Acknowledgement

The authors acknowledge the financial support from the Slovenian Research Agency (Research Core Funding No. P2-0190, Grant numbers 1000-20-0552, 6316-3/2018-255, 603-1/2018-16), as well as from the Metrology Institute of the Republic of Slovenia (funding of national standard of length; Contract No. C3212-10-000072). Furthermore, the authors would like to acknowledge the use of research equipment for processing and monitoring the machining and forming processes: Laser measuring systems for machine tools and coordinate measuring machines, procured within the project "Upgrading national research infrastructures - RIUM", which was co-financed by the Republic of Slovenia, the Ministry of Education. This specific research was also a part of the national project No. V2-24074 within the framework of the Targeted Research Program "CRP 2024" and the European project 23IND08-Di-Vision within the framework of the European Partnership on Metrology. Therefore, we would also like to acknowledge the support of the Slovenian Research Agency, Ministry of the Economy, Tourism and Sport, and the European Commission.

References

[1] Hermann G and Rudas I, Calibration system for tactile measuring probes, *SISY 2015 – IEEE, 13th Int. Symp. Intell. Syst. Informatics, Proc.*, pp. **145–148**, 2015

[2] Peingbangyang S and Wongsaroj J, Characteristics of Linear Variable Differential Transformer(LVDT) Probe for Gauge Blocks Calibration, *J. Phys. Conf.Ser.*, vol. **901**, 2017

[3] C Lipus L, Acko B, and Tompa J, Experimental determination of influences on a gauge block's stack length, *Adv. Prod. Eng. Manag.*, vol. **17**, 2022

[4] Ma Z, Choi J, and Sohn H, Structural displacement sensing techniques for civil infrastructure: A review, *J. Infrastruct. Intell. Resil.*, vol. **2**, 2023

[5] Byman V, Jaakkola T, Palosuo I, and Lassila A, High accuracy step gauge interferometer, Meas. Sci. Technol., vol. **29**, 2018

[6] Stoup J and Faust B, Measuring Step Gauges Using the NIST M48 CMM, *NCSLI Meas.*, vol. **6**, 2011

[7] Zhang L, Li J, Wu Y, Zhang K, Wang Y, Prediction model and experimental validation for the thermal deformation of motorized spindle, *Heat Mass Transf Und Stoffuebertragung*, **54**, 2018

[8] Naumann A, Ruprecht D, Wensch J, Toward transient finite element simulation of thermal deformation of machine tools in real-time *Comput Mech*, **62**, 2018

[9] Zheng E, Yang Y, Peng Z, Zhu Y, Zhao X, Lin X and Kang M, Thermal characteristics analysis and error prediction for lubricated multi-link high-speed precision presses, *J Mech Sci Technol*, **33**, 2019

[10] Šafarič J, Dolšak B, Klobučar R, Ačko B, Analysis of thermal contribution to the measurement uncertainty in step gauge calibration, *Precision Engineering*, **66**, 2022

[11] Chenyang Z, Cheng C and Hang Z, Study on nonlinear thermal error of the measurement machine, *IEEE 2011 10th International Conference on Electronic Measurement & Instruments*, Chengdu, China, 2011